

# Capillary Condensation and Interface Structure of a Model Colloid-Polymer Mixture in a Porous Medium

Paul P. F. Wessels\*

*Institut für Theoretische Physik II, Heinrich-Heine-Universität Düsseldorf,  
Universitätsstraße 1, 40225 Düsseldorf, Germany*

Matthias Schmidt†

*Debye Institute, Utrecht University, Princetonplein 5, 3584 CC Utrecht, The Netherlands*

Hartmut Löwen

*Institut für Theoretische Physik II, Heinrich-Heine-Universität Düsseldorf,  
Universitätsstraße 1, 40225 Düsseldorf, Germany*

(Dated: October 29, 2018)

We consider the Asakura-Oosawa model of hard sphere colloids and ideal polymers in contact with a porous matrix modeled by immobilized configurations of hard spheres. For this ternary mixture a fundamental measure density functional theory is employed, where the matrix particles are quenched and the colloids and polymers are annealed, i.e. allowed to equilibrate. We study capillary condensation of the mixture in a tiny sample of matrix as well as demixing and the fluid-fluid interface inside a bulk matrix. Density profiles normal to the interface and surface tensions are calculated and compared to the case without matrix. Two kinds of matrices are considered: (i) colloid-sized matrix particles at low packing fractions and (ii) large matrix particles at high packing fractions. These two cases show fundamentally different behavior and should both be experimentally realizable. Furthermore, we argue that capillary condensation of a colloidal suspension could be experimentally accessible. We find that in case (ii), even at high packing fractions, the main effect of the matrix is to exclude volume and, to high accuracy, the results can be mapped onto those of the same system without matrix via a simple rescaling.

## I. INTRODUCTION

Bringing a fluid in contact with a porous medium has a profound influence on its characteristics and phase behavior [1, 2]. Due to abundance of surfaces and their necessary proximity, surface-fluid interactions as well as capillarity effects play a prominent role. Moreover, the system may be trapped in locally stable states, and its behavior governed by hysteresis. Apart from the above fundamental questions, the study of adsorbates in porous media is also of great interest in applied fields ranging from industrial and geophysical to biomedical and pharmaceutical systems [2, 3].

Many natural porous materials are tremendously complex on a microscopic scale: irregularly shaped pores build a connected void space that percolates throughout the sample [4, 5]. In contrast, to facilitate systematic studies, one often relies on model pores like slit-like, cylindrical or spherical pores (see [1, 2] and Refs. therein). The pore is then described conveniently in terms of a single parameter, its size. A different class of idealized system makes use of immobilized arrangements of fluid particles (i.e. a quenched hard sphere fluid) to

model a porous medium (see [2] and Refs. therein). In turn, this is characterized through its density and the size of the spheres. However, the relevant difference to idealized pores is the presence of *random* confinement.

The study of porous media has been focused so far mainly on atomic liquids. In a colloidal fluid, length and time scales are much larger, facilitating e.g. studies in real space and time [6]. We believe that the use of colloidal suspensions as model systems to study the behavior of adsorbates in porous media can be as beneficial as their use to study many other phenomena in condensed matter. However, the experimental challenge lies in constructing three-dimensional porous media suitable for colloidal suspensions.

Colloidal porous media in 2D have been prepared by Cruz de León et. al. [7, 8] by confining a suspension of large colloids between parallel glass plates. Then, these served as a porous matrix to a fluid of smaller particles which remained mobile and of which they measured the structure and effective potentials. To our knowledge, no experiment similar in spirit has been performed in three dimensions to date. On the other hand, Kluijtmans et. al. constructed 3D porous glasses of silica spheres [9, 10] and silica rods [11], but studied the dynamics of isolated tracer colloids in these media. Weroński et al. studied transport properties in porous media of glass beads [12]. Still, such glassy arrangements of spherical colloids are a direct candidate for porous media suitable for colloidal suspensions. Sediments of large and heavy colloids as used in Refs [9, 10, 12] could be brought in contact

\*Electronic address: wessels@thphy.uni-duesseldorf.de

†On leave from: Institut für Theoretische Physik II, Heinrich-Heine-Universität Düsseldorf, Universitätsstraße 1, 40225 Düsseldorf, Germany

with a suspension of smaller density-matched (to the solvent) colloids of which the local structure could be determined [7, 8]. However, the size ratio of the two species is a crucial control parameter: It has to be large enough ( $\gtrsim 10$ ) such that the small particles can penetrate the void space, but should still be small enough such that no complete separation of length scales occurs. Another way to realize such porous media would be to use laser tweezers. In a binary colloid mixture of which one of the species possesses the same index of refraction as the solvent (via index-matching) and the other type has a higher index of refraction the second species could be trapped while the first would still remain mobile. Using multiple traps at random positions in space (mimicking a fluid) one could then realize a model porous matrix [13]. The advantages of this method are the accessibility of very low matrix packing fractions and the full control of the confinement. However, the number of trapped colloids in such setups is typically limited to the order of 100 – probably too little to approach real macroscopic porous media, but in the right regime to be able to compare to computer simulations, where similar numbers are accessible. The crucial advantage of these setups over the use of “natural” porous media is their model character arising from the use of well-defined monodisperse matrix spheres, while these still possess the essential features of random confinement and a highly interconnected void structure.

One prominent phenomenon that is induced by confinement is capillary condensation: A liquid inside the porous medium is in equilibrium with its vapor outside the medium. In order for a substance to phase separate into a dense liquid and a dilute gas phase a sufficiently long-ranged and sufficiently strong attraction between the constituting particles is necessary. It is well-known that the addition of non-adsorbing polymers to a colloidal dispersions induces an effective attraction between the colloids. The polymer coils are depleted from a shell around each colloid and overlap of these (depletion) shells generates more available volume to the polymers yielding an effective attraction between the colloids. Consequently, these colloid-polymer mixtures may separate into a colloid-poor (gas) phase and a colloid-rich (liquid) fluid [14].

The most simplistic theoretical model that has been applied for the study of such colloid-polymer mixture is the Asakura-Oosawa (AO) model [15, 16, 17] that takes the colloids to be hard spheres and the polymers to be ideal spheres that are excluded from the colloids. The bulk phase behavior of this model was studied with a variety of techniques, like effective potentials [18, 19], free volume theory [20], density functional theory (DFT) [21, 22] and simulations [19, 23, 24]. Recent work has also been devoted to inhomogeneous situations, i.e. the free interface between demixed fluid phases [25, 26, 27, 28], the adsorption behavior at a hard wall, where in particular a novel type of entropic wetting was found [24, 27, 28] and the behavior in spatially peri-

odic external potentials [29]. The surface tension between demixed colloid-polymer systems has been measured experimentally and established to be much lower than for atomic systems [30, 31, 32, 33]. Further, recent experiments confirm wetting of the colloid-rich liquid at a hard wall [34, 35].

DFT [36] can be used in two ways to treat adsorbates in porous media. The first is the (conceptually) straightforward approach via treating the porous medium as an external potential (see e.g. Refs. [37, 38, 39]) and to solve for the one-body density distributions of the fluid species. Those can be complicated spatial distributions, hence this approach is computationally demanding, but also yields information on out-of-equilibrium behavior like hysteresis in ad- and desorption curves [40, 41, 42].

A recently proposed alternative is to describe the quenched component on the level of its one-body density distribution [43]. Following the fundamental measure theory (FMT) of hard spheres [44, 45, 46], an explicit scheme was obtained to generate an approximate excess free energy for (not necessarily additive) hard-sphere mixtures in contact with hard-sphere matrices [43]. Applied to the AO model, the results were compared with those from solving the so-called replica Ornstein-Zernike (ROZ) equations [47, 48, 49, 50] and found to be in good agreement [51]. Meanwhile, this quenched-annealed (QA) DFT has been compared to computer simulations [52] and extended to hard-rod matrices [53] and lattice fluids [54, 55]. FMT in combination with mean field theory has also been applied to fluids inside model pores [56, 57].

In this article, we revisit the AO model in contact with a hard-sphere matrix using the QA DFT of Refs. [43, 51]. We study capillary condensation in a tiny sample of matrix as well as the fluid-fluid interface inside a bulk matrix. For both these phenomena, we distinguish two cases of matrices: (i) matrix particles having the same size as the colloids and (ii) where they are much larger. These correspond to the two possible experimental realizations we discussed earlier in the introduction, but also serve as representative cases because their behavior is fundamentally different. Concerning capillary condensation, we focus on the possible experimental realization and consider a bulk mixture in contact with in tiny sample of matrix. Furthermore, we elaborate if and how capillary condensation could be observable in such experiments. Concerning the fluid-fluid interface, we study the interfacial profiles as well as the surface tensions inside the matrix. For the case of small matrix particles (i), we determine the nature of decay (monotonic or periodic) of the interfaces which we compare with the bulk pair correlations. For the case of large matrix particles (ii), we observe a simple rescaling of the bulk as well as the interface results with respect to the case without matrix. Inhomogeneous situations like the fluid-fluid interface, are treated within QA DFT in a direct fashion, in contrast to e.g. the ROZ equations. Fluid-fluid interfaces have been studied before in Lennard-Jones systems in contact

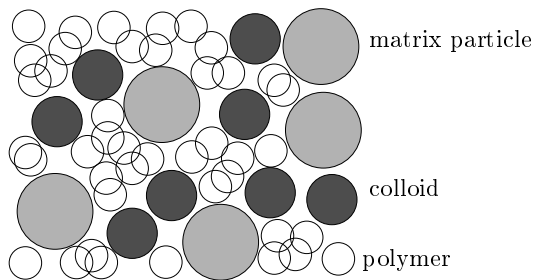


FIG. 1: Sketch of the ternary mixture of mobile colloids (dark), mobile polymers (transparent) and immobile matrix particles (grey). The polymer coils can freely overlap. There are three model parameters, i.e. the packing fraction of matrix particles,  $\eta_m$  and two size ratios,  $q = R_p/R_c$  and  $s = R_m/R_c$  where  $R_i$  are the radii of particles of species  $i$ . The packing fractions of colloids and polymers,  $\eta_c$  and  $\eta_p$  respectively, are the thermodynamic parameters.

with porous media using the Born-Green-Yvon equation as well as computer simulations [58, 59] and we briefly compare to results of our profiles.

The paper is organized as follows. In Sec. II we define our theoretical model explicitly. The QA DFT approach is reviewed in Sec. III, and the results are presented in Sec. IV. We first consider capillary condensation in a tiny sample and then demixing, the interfacial profiles and tensions inside a matrix. We conclude with a discussion in Sec. V.

## II. MODEL

We consider a three-component mixture of colloids (denoted by  $c$ ), polymers ( $p$ ) and immobile matrix particles ( $m$ ). Each of these particles are spherical objects with radii  $R_i$  and  $i = c, p, m$  and corresponding number densities  $\rho_i = N_i/V$  where  $N_i$  is the total number of molecules of species  $i$  and  $V$  is the system volume. All of these components are modeled as hard bodies meaning they cannot overlap but otherwise do not interact with each other, except for the polymer-polymer interaction, which is taken to be ideal, see Fig. 1. Consequently when  $r$  is the mutual distance, the pair potentials become

$$u_{ij}(r) = \begin{cases} \infty & \text{if } r < R_i + R_j \\ 0 & \text{if } r \geq R_i + R_j \end{cases} \quad (1)$$

for  $i, j = c, p, m$  except for  $i = j = p$

and concerning the polymer-polymer interaction, this simply becomes

$$u_{pp}(r) = 0 \quad \text{for all } r. \quad (2)$$

As all interactions are either hard-core or ideal, the (phase) behaviour is governed by entropic (packing) effects and the temperature  $T$  does not play a role. The only thermodynamic parameters are the colloid and

polymer packing fractions  $\eta_c = 4\pi R_c^3 \rho_c/3$  and  $\eta_p = 4\pi R_p^3 \rho_p/3$ , respectively. The remaining model parameters are two size ratios  $q = R_p/R_c$  and  $s = R_m/R_c$  and the packing fraction of matrix particles  $\eta_m = 4\pi R_m^3 \rho_m/3$ . It has to be mentioned that due to the fact that the polymers can freely overlap, the ‘‘polymer packing fraction’’ can easily be larger than one (Fig. 1). The mixture of hard spheres with these last-mentioned ideal polymers (i.e. without the matrix particles) is called the Asakura-Oosawa (AO) mixture [15, 16].

## III. DENSITY FUNCTIONAL THEORY

### A. Zero-Dimensional Limit

In this subsection we derive the zero-dimensional (0D) Helmholtz free energy for the three-component system of the AO colloid-polymer mixture in contact with quenched hard spheres. This 0D free energy is used as an input to construct the fundamental measure theory in the next subsection. Here, we give only a brief derivation, a more extensive version with more comments is given in Refs. [43, 51]. The essential ingredient is that we need to perform the so-called ‘‘double average’’ which refers to the statistical average over all fluid configurations and subsequently over all matrix realizations. To that end we consider a 0D cavity which either does or does not contain a matrix particle. Hence, the 0D partition sum is that of a simple hard sphere fluid,

$$\bar{\Xi}_m = 1 + \bar{z}_m, \quad (3)$$

where  $\bar{z}_m = \zeta \exp(\beta \bar{\mu}_m)$  is the fugacity of the hard spheres. Further,  $\beta = 1/k_B T$  with  $k_B$  Boltzmann’s constant and  $\bar{\mu}_m$  the chemical potential. The irrelevant prefactor  $\zeta$  scales with the vanishing volume of the cavity but has no effect to the final free energy and will not be discussed further. In general, we use an overbar to refer to quantities of 0D systems. With the grand potential,  $\beta \bar{\Omega}_m = -\ln \bar{\Xi}_m$ , the average number of matrix particles is  $\bar{\eta}_m = -\bar{z}_m \partial \beta \bar{\Omega}_m / \partial \bar{z}_m = \bar{z}_m / (1 + \bar{z}_m)$ .

Next, we consider the colloid-polymer mixture in contact with the matrix in zero dimensions. If the cavity is occupied by a matrix particle, no colloid or polymer can be present. On the other hand, if there is no matrix particle, it can either be empty, occupied by a single colloid or an arbitrary number of polymers. Hence,

$$\bar{\Xi} = \begin{cases} 1 & \text{matrix particle in cavity} \\ \bar{z}_c + \exp(\bar{z}_p) & \text{no matrix particle in cavity} \end{cases}, \quad (4)$$

where  $\bar{z}_c$  and  $\bar{z}_p$  are the colloid and polymer fugacities respectively. Then, the contribution  $-\ln \bar{\Xi}$  to the grand potential should contain the appropriate statistical weight for each of the cases, i.e.  $\bar{z}_m / \bar{\Xi}_m$  for the first and  $1 / \bar{\Xi}_m$  for the second,

$$\beta \bar{\Omega} = -\frac{\ln(\bar{z}_c + \exp(\bar{z}_p))}{1 + \bar{z}_m}. \quad (5)$$

Average particle numbers are again readily obtained via  $\bar{n}_i = -\bar{z}_i \partial \beta \bar{\Omega} / \partial \bar{z}_i$  for  $i = c, p$  (not for  $m$ ). The Helmholtz free energy can then be calculated using a standard Legendre transformation,  $\beta \bar{F} = \beta \bar{\Omega} + \sum_{i=c,p} \bar{n}_i \ln(\bar{z}_i)$  and we obtain for the excess part,  $\beta \bar{F}_{\text{exc}} = \beta \bar{F} - \sum_{i=c,p} \bar{n}_i [\ln(\bar{n}_i) - 1]$ ,

$$\beta \bar{F}_{\text{exc}}(\bar{n}_c, \bar{n}_p; \bar{n}_m) = (1 - \bar{n}_c - \bar{n}_p - \bar{n}_m) \ln(1 - \bar{n}_c - \bar{n}_m) + \bar{n}_c - (1 - \bar{n}_m) \ln(1 - \bar{n}_m). \quad (6)$$

This result can be shown to be equal from that which would be obtained using the so-called ‘‘replica trick’’ [50].

## B. Fundamental Measure Theory

Fundamental measure theory (FMT) is a nonlocal density functional theory, in which the excess part of the *three-dimensional* free energy  $F_{\text{exc}}$  is expressed as a spatial integral over the free energy density  $\Phi$ ,

$$\beta F_{\text{exc}}[\{\rho_i(\mathbf{r})\}] = \int d\mathbf{r} \Phi(\{n_\nu^i(\mathbf{r})\}). \quad (7)$$

This free energy density in turn is assumed to depend on the full set of weighted densities  $\{n_\nu^i(\mathbf{r})\}$ ,

$$\begin{aligned} n_\nu^i(\mathbf{r}) &= \int d\mathbf{r}' w_\nu^i(\mathbf{r} - \mathbf{r}') \rho_i(\mathbf{r}'), \\ &= (w_\nu^i \otimes \rho_i)(\mathbf{r}) \end{aligned} \quad (8)$$

which are convolutions (denoted with  $\otimes$ ) with the single-particle distribution functions  $\rho_i(\mathbf{r})$  for species  $i = c, p, m$ . The weight functions are obtained from the low-density limit where the virial series has to be recovered,

$$\begin{aligned} w_3^i(\mathbf{r}) &= \theta(R_i - r) \\ w_2^i(\mathbf{r}) &= \delta(R_i - r) & \mathbf{w}_{v2}^i(\mathbf{r}) &= \delta(R_i - r) \mathbf{r} / r \\ w_1^i(\mathbf{r}) &= \delta(R_i - r) / (4\pi r) & \mathbf{w}_{v1}^i(\mathbf{r}) &= \delta(R_i - r) \mathbf{r} / (4\pi r^2) \\ w_0^i(\mathbf{r}) &= \delta(R_i - r) / (4\pi r^2) \end{aligned} \quad (9)$$

with again  $i = c, p, m$  being one of the three components  $\theta$  the Heaviside function and  $\delta$  the Dirac delta function. There are four scalar weight functions, with 3 to 0, corresponding respectively to the volume of the particles, the surface area, the mean curvature and the Euler characteristic and these are the so-called ‘‘fundamental measures’’ of the sphere. The two weights on the right-hand side of Eq. 9 are vector quantities. Often a seventh tensorial weight is used in the context of freezing but this will not be used here [21, 22, 46]. The dimensions of the weight functions  $w_\nu^i$  are  $(\text{length})^{\nu-3}$ .

Then, the sole approximation made is that  $\Phi$  is taken to be a *function* of the weighted densities  $n_\nu^i(\mathbf{r})$  whereas most generally one would expect this to be a *functional* dependence. This approximation totally sets the form of  $\Phi$  and following Refs. [22, 43, 51] we give the expression

for  $\Phi = \Phi_1 + \Phi_2 + \Phi_3$  in terms of the zero-dimensional free energy derived in the previous subsection,

$$\Phi_1 = \sum_{i=c,p,m} n_0^i \varphi_i(\{n_3^l\}), \quad (10)$$

$$\Phi_2 = \sum_{i,j=c,p,m} \left( n_1^i n_2^j - \mathbf{n}_{v1}^i \cdot \mathbf{n}_{v2}^j \right) \varphi_{ij}(\{n_3^l\}), \quad (11)$$

$$\Phi_3 = \frac{1}{8\pi} \sum_{i,j,k=c,p,m} \left( \frac{1}{3} n_2^i n_2^j n_2^k - n_2^i \mathbf{n}_{v2}^j \cdot \mathbf{n}_{v2}^k \right) \varphi_{ijk}(\{n_3^l\}) \quad (12)$$

with

$$\varphi_{i_1 \dots i_t}(\{\bar{n}_j\}) = \partial^t \beta \bar{F}_{\text{exc}}(\{\bar{n}_j\}) / \partial \bar{n}_{i_1} \dots \partial \bar{n}_{i_t}. \quad (13)$$

All  $\varphi_{i_1 \dots i_t}$  of which more than one indices equal  $p$  are zero due to the form of  $\beta \bar{F}_{\text{exc}}$ . Together, Eqs. (6) to (13) constitute the excess free energy functional for this QA system.

## C. Minimization

Having constructed the excess free energy, we can now immediately move on to the the grand-canonical free energy functional of the colloid-polymer mixture in contact with a matrix,

$$\begin{aligned} \Omega[\rho_c(\mathbf{r}), \rho_p(\mathbf{r}); \rho_m(\mathbf{r})] &= F_{\text{exc}}[\rho_c(\mathbf{r}), \rho_p(\mathbf{r}); \rho_m(\mathbf{r})] + \\ &+ k_B T \sum_{i=c,p} \int d\mathbf{r} \rho_i(\mathbf{r}) [\ln(\rho_i(\mathbf{r}) \Delta_i) - 1] + \\ &+ \sum_{i=c,p} \int d\mathbf{r} \rho_i(\mathbf{r}) [V_i(\mathbf{r}) - \mu_i] \end{aligned} \quad (14)$$

Here,  $\Delta_i$  is the ‘‘thermal volume’’ which is the product of the relevant de Broglie wavelengths of the particles of species  $i$ . Further,  $\mu_i$  is the chemical potential and  $V_i$  is the (external) potential acting on component  $i$ . In this paper, we study bulk phase behaviour and the free fluid-fluid interfaces so we use  $V_i = 0$ . The equilibrium profiles are the ones that minimize the functional,

$$\frac{\delta \Omega}{\delta \rho_c(\mathbf{r})} = 0 \quad \text{and} \quad \frac{\delta \Omega}{\delta \rho_p(\mathbf{r})} = 0. \quad (15)$$

This yields the Euler-Lagrange or stationarity equations ( $i = c, p$ ),

$$\rho_i(\mathbf{r}) = z_i \exp \left[ c_i^{(1)}(\{\rho_j(\mathbf{r})\}) \right], \quad (16)$$

with  $z_i = \Delta_i^{-1} \exp[\beta \mu_i]$  the fugacity of component  $i$  and the one-particle direct correlation functions given by

$$c_i^{(1)}(\mathbf{r}) = -\beta \frac{\delta F_{\text{exc}}[\{\rho_j(\mathbf{r})\}]}{\rho_i(\mathbf{r})} = -\sum_\nu \left( \frac{\partial \Phi}{\partial n_\nu^i} \otimes w_\nu^i \right) (\mathbf{r}) \quad (17)$$

Obviously, the functional is not minimized with respect to the matrix distribution  $\rho_m(\mathbf{r})$  as this serves as an *input* profile. In principle, as we are dealing with a quenched-annealed system in which the matrix is initially (before quenching) a hard sphere fluid,  $\rho_m(\mathbf{r})$  should still minimize the hard sphere functional [43, 51]. However, as density functional theory allows us to generate any distribution  $\rho_m(\mathbf{r})$  by applying any suited external potential (which we can then remove after quenching), we do not need to go into the scheme of generating matrix profiles. Moreover, in the present paper we use fluid distributions of the matrix particles which minimize (at least locally) the hard sphere functional without external potential for any packing fraction.

#### IV. RESULTS

In this section, we show results of the effect of the hard sphere matrix on the AO colloid-polymer mixture concerning capillary condensation in a tiny sample of matrix, and phase behaviour and free fluid-fluid interfaces inside a bulk matrix. Throughout this section, we distinguish between the colloid-sized matrix particles ( $s = 1$ ) and the large matrix particles (we use  $s = 50$ ). In the first case, as we will see, one is limited to small matrix packing fractions (up to  $\eta_m$  of the order of 0.2) as for high packing fractions the pores become too small for the colloids and the polymers to constitute a real fluid in the matrix. For the large matrix particles, higher matrix packing fractions are accessible (up to  $\eta_m = 0.5$ ). Finally, in all cases we use  $q = 0.6$ , for which size ratio the AO model has a stable fluid-fluid demixing area (with respect to freezing, which we do not consider).

##### A. Bulk Fluid Free Energy

In the fluid phase, the densities are spatially homogeneous, and the constant distributions  $\rho_i(\mathbf{r}) = \rho_i$  solve the stationarity Eqs. (16) and (17). Therefore, we only have to integrate the weights over space,  $\int d\mathbf{r} w_v^i$ , and the weighted densities become

$$\begin{aligned} n_3^i &= \eta_i, \\ n_2^i &= 3\eta_i/R_i, \\ n_1^i &= 3\eta_i/(4\pi R_i^2), \\ n_0^i &= 3\eta_i/(4\pi R_i^3), \\ \mathbf{n}_{v2}^i &= \mathbf{n}_{v1}^i = 0, \end{aligned} \quad (18)$$

with  $i = c, p, m$ . Substituting these expressions in the free energy density, Eq. (10) to (12) we obtain an analytical expression for the bulk excess free energy. Defining the dimensionless bulk free energy density,  $f = \beta F V_c / V$

with  $V_c = 4\pi R_c^3/3$  the volume of a colloid, this becomes

$$\begin{aligned} f(\eta_c, \eta_p; \eta_m) &= \eta_c (\ln \eta_c - 1) + \frac{\eta_p}{q^3} (\ln \eta_p - 1) \\ &\quad + f_0(\eta_c, \eta_m) - \frac{\eta_p}{q^3} \ln \alpha(\eta_c, \eta_m) \end{aligned} \quad (19)$$

with the last two terms being the excess free energy. We have separated the excess free energy in two terms where  $f_0$  the excess free energy density of a fluid of hard spheres in contact with a hard sphere matrix and  $\alpha$  is the fraction of free volume for the polymers in the presence the hard sphere colloidal fluid *and* the hard sphere matrix [20, 22]. The expressions for  $f_0$  and  $\alpha$  are quite extensive and given in the appendix. In going from Eq. (7) to (19) we have discarded two terms,  $\eta_c \ln(\Delta_c/V_c)$  and  $(\eta_p/q^3) \ln(\Delta_p/V_p)$ , linear in the colloid and polymer packing fractions. These have no effect on the phase behaviour. Due to the ideal interactions of the polymers, the excess free energy density is only linear in  $\eta_p$  and the polymer fugacity becomes simply

$$z_p V_p = \eta_p / \alpha(\eta_c, \eta_m). \quad (20)$$

This relation is trivially invertible, so switching from system representation (using  $f(\eta_c, \eta_p; \eta_m)$ ) to the polymer reservoir representation (in terms of  $\tilde{\omega}(\eta_c, z_p; \eta_m) = f - \mu_p \eta_p / q^3$ ) is straightforwardly done. Moreover, for zero packing fractions of colloids and matrix particles, the polymer free volume fraction is trivial,  $\alpha(0, 0) = 1$ . Consequently, the fugacity equals the packing fraction of polymers in the polymer reservoir,  $z_p V_p = \eta_{p,r}$  (where there are no colloids and matrix particles), and often, we use  $\eta_{p,r}$  when referring to the fugacity. Finally, we mention that in the absence of matrix particles,  $\eta_m = 0$ , this theory is equivalent to the free-volume theory for the AO model [20, 21, 22].

Concerning the fluid-fluid demixing, the spinodals are calculated in the canonical representation, by solving  $\det[\partial^2 f / \partial \eta_i \partial \eta_j] = 0$  with  $i, j = c, p$ , which can be done analytically. Binodals are determined by constructing the common tangents of the semi-grand potential  $\tilde{\omega}(\eta_c, \eta_{p,r}; \eta_m)$  at fixed fugacity  $\eta_{p,r}$ .

When the matrix particles are very large, it is expected that the excluded volume effects dominate over other (surface or capillary) effects. In particular, if one considers only one infinitely large particle, still corresponding to a nonzero matrix packing fraction, one would expect normal bulk behavior of the mixture as most of the mixture is “far” away from the matrix particle. Equivalently, for very large matrix particles, the total volume of the surrounding depletion layers, which are responsible for the surface effects, compared to the actual volume occupied by the matrix particles scales with  $(4\pi(R_m + R_c)^3 \rho_m / 3 - \eta_m) / \eta_m \propto 3/s$  for the colloids and  $(4\pi(R_m + R_p)^3 \rho_m / 3 - \eta_m) / \eta_m \propto 3q/s$  for the polymers, and these both go to zero for  $s \rightarrow \infty$ . However, in this limit, we still need to correct for the volume as this is partly occupied by infinitely large matrix particles, i.e.

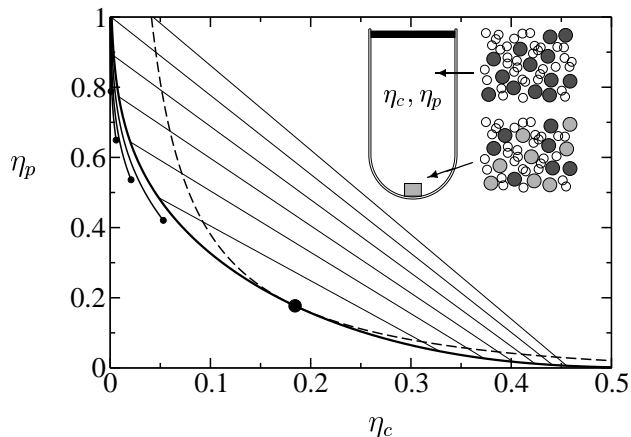


FIG. 2: Phase diagram of a bulk AO colloid-polymer mixture ( $q = 0.6$ ) in chemical contact with a tiny sample of porous material ( $s = 1$ ). Concerning the bulk mixture: the thick full curve is the binodal, the dashed is the spinodal, the large filled circle (where they meet) is the critical point and the straight (thin) lines are the tie lines connecting coexisting state points. The capillary lines (full curves) appear in the upper left (colloid-poor) part of the phase diagram and each terminates in a capillary critical point (small filled circles). From lower-right to upper-left, the curves correspond to an increasing packing fraction of the matrix,  $\eta_m = 0.05, 0.1, 0.15, 0.2$  (the last one is practically on the vertical axis near  $\eta_p = 0.8$ ). The inset shows a sketch of the setup: a test tube is sealed at the top and filled with the colloid-polymer mixture (densities  $\eta_c$  and  $\eta_p$ ) and at the bottom lies the tiny sample of porous matrix.

$V \rightarrow (1 - \eta_m)V$ . Indeed, applying  $s \rightarrow \infty$  to the bulk free energy of Eq. (19), we re-obtain the bulk behaviour of the plain AO colloid-polymer mixture *without* matrix, i.e. it can be shown that

$$\lim_{s \rightarrow \infty} f(\eta_c, \eta_p; \eta_m) = (1 - \eta_m) f\left(\frac{\eta_c}{1 - \eta_m}, \frac{\eta_p}{1 - \eta_m}; 0\right), \quad (21)$$

where the free energy density has to be rescaled as well. This term can be considered to be the zeroth in a  $1/s$ -expansion of the free energy of which higher order terms should correspond to effects due to surfaces, capillarity, curvature etc. However, because of the formidable form of the free energy it is a daunting task to connect every term to a certain phenomenon and we leave this to future investigation. It is worth mentioning that a power series in  $1/s$  is only a simple model dependence. In general, there can be non-analyticities, e.g. arising from wetting phenomena around curved surfaces [60] of matrix particles.

### B. Capillary Condensation in a Tiny Sample of Porous Matrix

A porous matrix of quenched hard spheres stabilizes the colloid-rich phase with respect to the colloidal gas

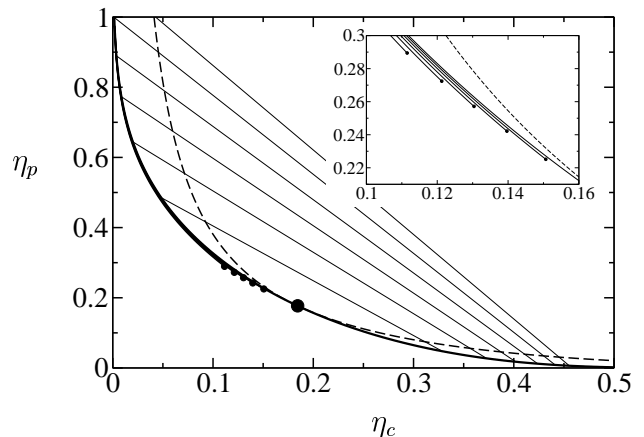


FIG. 3: Same as in Fig. 2, but now for a sample of porous matrix with  $s = 50$ . Here the matrix packing fractions increase as follows:  $\eta_m = 0.1, 0.2, 0.3, 0.4, 0.5$  (again from lower-right to upper-left). The inset is the magnification of the area with the capillary critical points.

phase [51]. This is called capillary condensation and it is due to the attractive depletion potential between the colloids, which also acts between colloids and matrix particles. In this subsection we present capillary condensation in a representation which is appropriate to compare with experiments. In an experimental setup one typically has a canonical ensemble, i.e. a test tube, of colloid-polymer mixture. By adding a tiny sample of porous material, the bulk mixture in the test tube acts as a colloid-polymer reservoir to the sample, but vice versa, if the sample is small enough, its state will not have any effect on that of the bulk mixture (see Fig. 2(inset)). In the colloid-poor (and polymer-rich) part of the phase diagram, on approaching bulk coexistence, the conditions for coexistence in the porous sample are reached before those in bulk, i.e. capillary condensation in the sample occurs. Hence, capillary condensation appears as a line in the system representation terminating in a capillary critical point. This is shown in Figs. 2 and 3 for the case of  $s = 1$  and  $s = 50$  respectively and various densities of the matrix. The coexistence of the bulk colloid-polymer mixture appears in the usual system representation, where tie lines connect coexisting states. For each of the matrix densities, a capillary line runs along the bulk binodal in the colloid-poor part of the phase diagram.

First, we determine the conditions for coexistence inside the matrix, i.e. we compute the combinations of chemical potentials  $\mu_{c,\text{coex}}^{\text{porous}}$  and  $\mu_{p,\text{coex}}^{\text{porous}}$ , for which demixing occurs within the porous sample. These are fixed by the chemical potentials of the bulk colloid-polymer mixture,  $\mu_c^{\text{bulk}}$  and  $\mu_p^{\text{bulk}}$ , so solving

$$\begin{aligned} \mu_c^{\text{bulk}}(\eta_c, \eta_p) &= \mu_{c,\text{coex}}^{\text{porous}}, \\ \mu_p^{\text{bulk}}(\eta_c, \eta_p) &= \mu_{p,\text{coex}}^{\text{porous}} \end{aligned} \quad (22)$$

for  $\eta_c$  and  $\eta_p$ , we obtain the capillary lines in the phase diagram in system representation. The trend can be

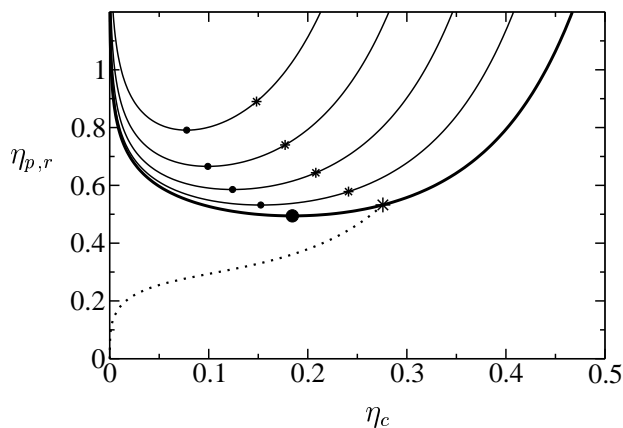


FIG. 4: Fluid-fluid binodals of an AO colloid-polymer mixture ( $q = 0.6$ ) inside a bulk porous matrix ( $s = 1$ ). The lines connecting coexisting state point are not drawn but run horizontal. The lower (thicker) curve is the result in the absence of any matrix,  $\eta_m = 0$ . For the other curves, the matrix packing fraction increases from bottom to top,  $\eta_m = 0, 0.05, 0.1, 0.15, 0.2$ . The filled circles are the critical points (large,  $\eta_m = 0$ ). The dotted line is the Fisher-Widom line for  $\eta_m = 0$  below of which the decay of correlations in the fluid is oscillatory and above these are monotonic. The point where the FW line hits the binodal is marked by a (large) star. The FW lines for the other matrix packing fractions are not shown, only their crossings with the binodals (small stars).

spotted from Figs. 2 and 3, increasing the matrix packing fraction in the sample, the capillary line moves away from the bulk binodal but at the same time the capillary critical point shifts away from the bulk critical point. Qualitatively this applies to both the  $s = 1$ - and  $s = 50$ -cases. However, in the  $s = 50$ -case the capillary lines extend to much closer to the bulk critical point, but they are hardly distinguishable from the bulk binodal. Concerning the colloid-sized matrix particles,  $s = 1$ , these capillary lines are well separated from the bulk binodal, but the capillary critical points are located much deeper into the colloidal gas regime.

Next, we briefly discuss the implications this has for possible experiments. Focusing on the case of the large matrix particles,  $s = 50$ , we take as an example  $\eta_m = 0.5$ . In this case the difference in chemical potential at coexistence of the mixture in bulk and inside the porous sample at constant polymer fugacity is of the order,  $\beta\Delta\mu_c^{\text{coex}} \sim 0.1$ , and it scales roughly with  $1/s$ . This difference is very small and brings up the question if this (i.e. capillary condensation) is observable in experiments. Typically, the effect of gravity is reduced by density-matching the colloids with the solvent, i.e. canceling gravity by means of buoyancy. However, this density-matching is never perfect, and the length scale  $(\beta m_c g)^{-1}$  is a measure for its success (at infinity it is perfect). Here  $g$  is the gravitational acceleration and  $m_c = (\rho_{\text{colloid}} - \rho_{\text{solvent}})V_c$  the effective mass of the colloid

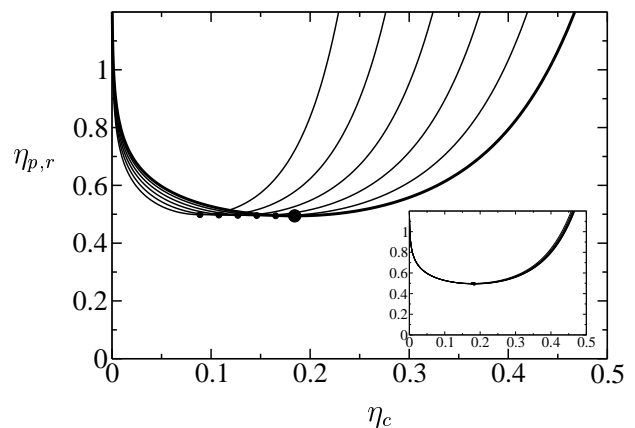


FIG. 5: Same as in Fig. 4, but now for  $s = 50$ . Matrix packing fractions increase from right to left,  $\eta_m = 0, 0.1, 0.2, 0.3, 0.4, 0.5$ . Inset: same curves now rescaled, i.e.  $\eta_{p,r}$  vs.  $\eta_c/(1 - \eta_m)$ .

in solution, with  $\rho_{\text{colloid}}$  and  $\rho_{\text{solvent}}$  the mass densities inside the colloid and of the solvent respectively. Therefore this length scale is strongly dependent on the colloid size,  $(\beta m_c g)^{-1} \propto R_c^{-3}$ , and can range from micrometers (large colloids) to meters (small colloids) in experiments [32]. Typically, polymers are much less sensitive to gravity as long as the solvent is good. When there is coexistence inside a test tube, there is only real coexistence at the liquid-gas interface whereas below and above the colloids have slightly different chemical potentials due to their gravitational energy. Consequently, moving upward from the interface, say  $\Delta z$ , the colloid chemical potential is  $(\beta m_c g)\Delta z$  lower than at coexistence. By placing the porous sample within  $\Delta z^* = \beta\Delta\mu_c^{\text{coex}}/(\beta m_c g)$  of the interface, capillary condensation should take place. Taking as an example,  $\beta\Delta\mu_c^{\text{coex}} \sim 0.1$  and  $(\beta m_c g)^{-1} \sim 1$  meter, it becomes clear that, within the context of this (idealized) model, values of  $\Delta z^* \sim 0.1$  meter should be accessible in experiments, meaning that capillary condensation could in principle be observed. Complete wetting of the large matrix spheres by the colloidal liquid may preempt capillary condensation close to the bulk critical point. Moving sufficiently far away from the critical point towards the dilute gas regime, the effects due to complete wetting should disappear while capillary condensation is retained.

### C. Phase Behaviour inside a Bulk Porous Matrix

We now return to the full ternary mixture in bulk, i.e. where in the previous subsection, the matrix was only a tiny sample immersed in a large system of colloid-polymer mixture, in this and the following subsections we consider the colloid-polymer mixture in a system-wide matrix. In this subsection, we revisit the demixing phase behavior which we need in the next subsections where we

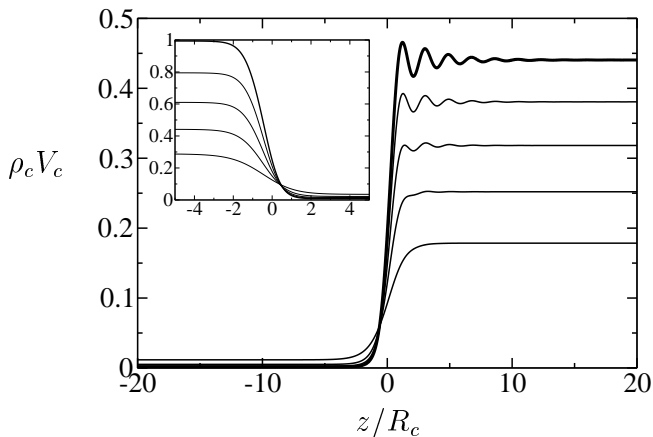


FIG. 6: Colloid density profiles ( $V_c = \frac{4}{3}\pi R_c^3$ ) normal to the free fluid-fluid interface for increasing matrix packing fractions at fixed polymer fugacity. Parameters are:  $q = 0.6$ ,  $s = 1$  and  $\eta_{p,r} = 1$  (see Fig. 4). The matrix packing fraction increases from top (thick profile,  $\eta_m = 0$ ) to bottom:  $\eta_m = 0, 0.05, 0.1, 0.15, 0.2$ . Inset: corresponding polymer profiles ( $\rho_p V_p$  vs.  $z/R_c$ , with  $V_p = \frac{4}{3}\pi R_p^3$ ) for the same values of the matrix packing fractions (also increasing from top to bottom).

study the fluid-fluid interface inside a matrix. Fig. 4 is the phase diagram in the polymer-reservoir representation for colloid-sized matrix particles,  $s = 1$ , for various matrix densities. Increasing the matrix packing fraction, there is less volume available to the colloids and the critical point shifts to smaller colloid packing fractions. At the same time, the porous matrix acts to keep the mixture “mixed” and therefore, the critical point shifts to higher polymer fugacities. For the case of  $s = 1$ , we can not go to much higher packing fractions than  $\eta_m \sim 0.2$  as then the critical fugacity shoots up dramatically to unphysically large values. This may be partly due to the relatively large depletion shells around the matrix particles which cause the pore sizes to become too small for the colloids and polymers to enter the matrix. In case of large matrix particles ( $s = 50$ , see Fig. 5), the latter effect is negligible and the pore sizes are always large enough. Consequently, only the excluded volume remains and rescaling the binodals with  $(1 - \eta_m)$  is very effective practically mapping the binodals onto each other, Fig. 5(inset). This rescaling is unsuccessful for  $s = 1$  as can be directly seen from the fact that the critical fugacities in Fig. 4 are different for each of the matrix densities.

In addition, we have determined the nature of the asymptotic decay of pair correlations of the fluid inside the matrix [61]. These can either be monotonic or periodic and the corresponding regions in the phase diagram are separated by the Fisher-Widom (FW) line, at which both types of decay are equally long-range. This line can be determined by studying the pole structure of the total correlation functions  $h_{ij}$  in Fourier space [61]. In the present case of QA systems, rather than using the usual

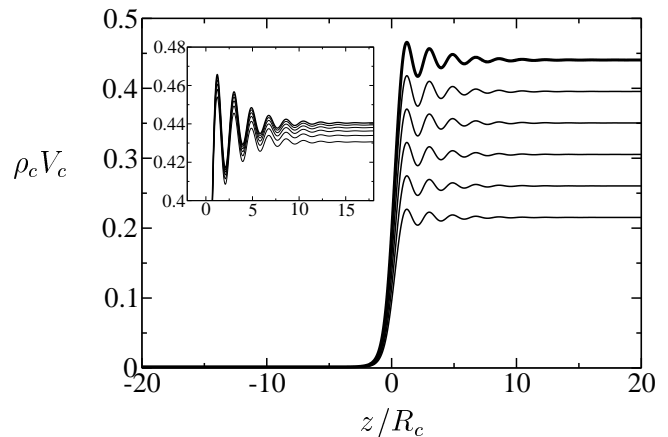


FIG. 7: Same as in Fig. 6 but now for  $s = 50$ . Other parameters are:  $q = 0.6$  and  $\eta_{p,r} = 1$  (see Fig. (5)). The matrix packing fractions increase from top (thick profile,  $\eta_m = 0$ ) to bottom:  $\eta_m = 0, 0.1, 0.2, 0.3, 0.4, 0.5$ . Inset: magnification of the rescaled profiles for the same curves, i.e.  $\rho_c V_c / (1 - \eta_m)$  vs.  $z/R_c$  (where again, matrix packing fractions increase from top to bottom).

Ornstein-Zernike equations, one has to use the replica-Ornstein-Zernike (ROZ) equations [50]. Neglecting correlations between the replicas, these are

$$h_{mm}(\mathbf{r}) = c_{mm}(\mathbf{r}) + \rho_m(c_{mm} \otimes h_{mm})(\mathbf{r})$$

$$h_{ij}(\mathbf{r}) = c_{ij}(\mathbf{r}) + \sum_{t=c,p,m} \rho_t(c_{it} \otimes h_{tj})(\mathbf{r}) \quad (23)$$

with  $i, j = c, p, m$  except  $i = j = m$ . Here, for  $ij \neq mm$ , the  $c_{ij}(\mathbf{r}) = -\delta^2 F_{\text{exc}} / \delta \rho_i(\mathbf{r}) \delta \rho_j(\mathbf{r})$  are the direct correlation functions for which we obtain analytic expressions by differentiating Eq. 7. The matrix structure is determined before the quench, so  $c_{mm}$  and  $h_{mm}$  are those of the normal hard sphere fluid at density  $\rho_m$  (Percus-Yevick-compressibility closure, see Refs. [43, 51]). This analysis follows closely that of Ref. [22] in which more details are given. In view of our subsequent interface study, we focus on the point where the FW line meets the binodal. In Fig. 4 ( $s = 1$ ), these are denoted by stars, and we observe that the shifts due to the matrices follow the same trend as the critical points. In case of  $s = 50$ , we have not determined the FW lines, but there is no reason to expect the simple rescaling of the case without matrix to fail in this case. Furthermore, concerning the density profiles (in the next subsection,  $s = 50$ ), we stay well within the oscillatory regime.

#### D. Fluid-Fluid Profiles inside a Bulk Porous Matrix

We have calculated density profiles at coexistence normal to the colloidal gas-liquid interface. In this case of planar interfaces, the density distribution is only a function of one spatial coordinate  $z$ ; i.e.  $\rho_i(\mathbf{r}) = \rho_i(z)$ .



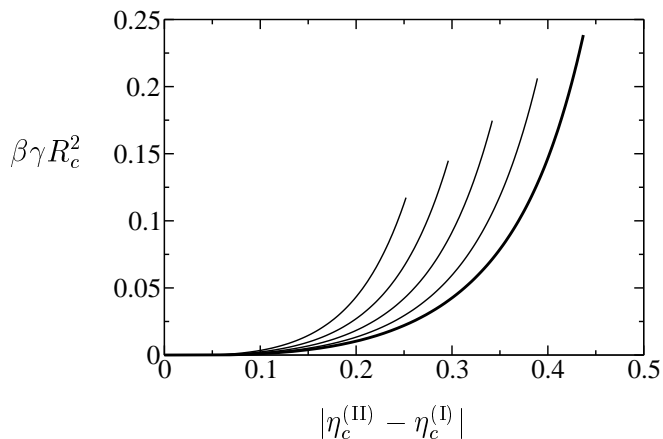


FIG. 8: Fluid-fluid surface tensions vs. the difference in colloid packing fractions of the two fluid phases for  $q = 0.6$ ,  $s = 1$  and various values of the matrix packing fraction. The matrix packing fractions increase from right ( $\eta_m = 0$ , thick curve) to left,  $\eta_m = 0, 0.05, 0.1, 0.15, 0.2$ . Each curve is computed from the critical point,  $\eta_{p,r} = \eta_{p,r}^{(\text{crit})}$  (where  $\gamma = 0$ ) until twice the critical fugacity,  $\eta_{p,r} = 2\eta_{p,r}^{(\text{crit})}$ .

The only dependence on the other two degrees of freedom is in the weights and this can be integrated out, to obtain projected weights,  $\tilde{w}_v^i(z) = \int dx dy w_v^i(\mathbf{r})$  (see e.g. [62]). The profiles are discretized and calculated via an iteration procedure, i.e. we insert profiles on the right hand side of Eq. (16) and then obtain new profiles on the left hand side, which are then reinserted on the right. Using step functions as iteration seeds, this procedure converges in the (local) direction of the lowest free energy. We normalize the densities as in bulk, i.e. we plot  $\rho_i(z)V_i$  so that  $\rho_i(\pm\infty)V_i = \eta_i^{(I,II)}$ , with I and II referring to the coexisting phases. The zero of  $z$  is set at the location of the interface, defined through the Gibbs dividing surface of the colloids:  $\int_{-\infty}^0 dz[\rho_c(z) - \rho_c(-\infty)] + \int_0^{\infty} dz[\rho_c(z) - \rho_c(\infty)] = 0$ .

In Figs. 6 and 7, we have plotted the colloid profiles normal to the interface for  $s = 1$  and  $s = 50$ , respectively. Colloid profiles are shown for increasing densities of the matrix at fixed fugacity,  $\eta_{p,r} = 1$ , corresponding to the bulk binodals in Figs. 4 and 5. For the case of  $s = 1$ , this means that, as the critical point shifts to higher fugacities, the profiles are effectively taken at fugacities closer to the critical value. We observe this well-known behavior in Fig. 6; close to the critical point the profiles are smoother and modulations less pronounced. Away from the critical point, the interface is sharp but the periodic modulations due to the surface extend to far in the bulk fluid. The inset of Fig. 6 shows the corresponding polymer profiles. In Ref. [58], the main result is that the interface widens due to the porous medium. The same happens here and is due to fact that one is effectively closer to the critical point.

In Fig. 7, as we saw for the bulk phase diagram, there is a simple rescaling at work and the profiles merely dif-

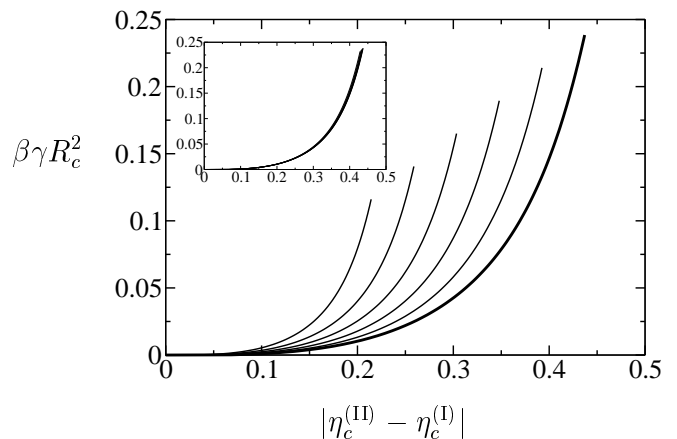


FIG. 9: Same as in Fig. 8 but now for  $s = 50$ . Again, matrix packing fractions increase from right ( $\eta_m = 0$ , thick curve) to left,  $\eta_m = 0, 0.1, 0.2, 0.3, 0.4, 0.5$ . Each curve is computed from the critical point,  $\eta_{p,r} = \eta_{p,r}^{(\text{crit})}$  (where  $\gamma = 0$ ) until twice the critical fugacity,  $\eta_{p,r} = 2\eta_{p,r}^{(\text{crit})}$ . Inset: the same (but rescaled) curves are shown, i.e.  $\beta\gamma R_c^2/(1 - \eta_m)$  vs.  $|\eta_c^{(II)} - \eta_c^{(I)}|/(1 - \eta_m)$ .

fer with a factor  $(1 - \eta_m)$ . The inset in Fig. 7 shows the same colloid profiles but now rescaled and we have zoomed in on the region close to the interface. Clearly, even the modulations follow the case without matrix with the same accuracy as the bulk coexistence values in the inset of Fig. 5.

We have also studied the asymptotic decay of correlations with the interface via the density profiles. These must be of the same nature as the decay of the direct correlations in bulk (determined via the ROZ equations, see previous subsection), i.e. either monotonic or periodic [61]. However, determining the crossing points of the FW line with the binodals using the interfacial profiles yields a systematic shift away from the critical point, compared to the bulk calculation ( $\sim 5\%$ ). Probably, this is due to numerical limits. Close to this crossing point both (the periodic and the monotonic) modes of decay are equally strong, so only far away from the interface truly asymptotic behavior may be observed. However, there, the periodic modulations may have become too small to be observable. Furthermore, our numerical routine has no real incentive to minimize the tails of the profiles as the gain in free energy is very low.

### E. Fluid-Fluid Surface Tension inside a Bulk Porous Matrix

The presence of the matrix also affects the surface tension between the colloidal liquid and gas phases. The interfacial or surface tension  $\gamma$  of planar interfaces in the grand canonical ensemble is defined through

$$\gamma A = \Omega_{\text{inh}} + PV \quad (24)$$

where  $A$  is the amount of surface area,  $\Omega_{\text{inh}}$  is the grand potential for the inhomogeneous system and  $P$  the pressure (i.e.  $-PV$  is the grand potential for the homogeneous bulk system). With our numerical scheme we calculate density profiles in  $z$ -direction so it makes sense to write the surface tension as an integral,

$$\gamma = \int dz [\omega(z) + P] \quad (25)$$

with

$$\begin{aligned} \omega(z) = & k_{\text{B}}T \sum_{i=c,p} \rho_i(z) [\ln(\rho_i(z)\Delta_i) - 1] \\ & - \sum_{i=c,p} \mu_i \rho_i(z) + k_{\text{B}}T \Phi(\{n_{\nu}^i(z)\}). \end{aligned} \quad (26)$$

The quantity  $\omega(z)$  is a “local” grand potential density whose average over space yields the actual grand potential per unit of volume  $\Omega_{\text{inh}}/V$ . In Figs. 8 and 9 we have plotted the surface tension versus the colloidal density difference in the two phases for  $s = 1$  and  $s = 50$ , respectively. In both cases the effect of the matrix is that the surface tensions increase faster with the difference  $|\eta_c^{(\text{II})} - \eta_c^{(\text{I})}|$  which is of course due to the fact that the coexistence area becomes less wide as the coexisting packing fractions themselves become smaller. In the inset of Fig. 9, we show the same curves rescaled with  $(1 - \eta_m)$ , and the rescaled graphs fall almost on top of the original one without any matrix. Here, we note that also the surface tension has been rescaled with  $(1 - \eta_m)$ ; this is needed from Eq. (21) as the free energy density  $\omega(z)$  needs to be rescaled as well. Again, this rescaling procedure is not successful for  $s = 1$ .

Often, the surface tension is plotted against the relative distance to the critical point,  $(\eta_{p,r}/\eta_{p,r}^{(\text{crit})} - 1)$  [27]. However, this does not improve the rescaling for  $s = 1$  and this can be seen from the fact that the end points of the curves in Figs. 8 and 9 are all at twice the critical fugacity,  $\eta_{p,r} = 2\eta_{p,r}^{(\text{crit})}$  and the surface tensions (rescaled or not) are at quite different values at the end points.

## V. CONCLUSION

We have considered the full ternary system of hard spheres and ideal polymers (represented by the AO model) in contact with a quenched hard sphere fluid acting as a porous matrix. Using a QA DFT in the spirit of Rosenfeld’s fundamental measure approach, we studied capillary condensation in a tiny sample of matrix as well as the fluid-fluid interface inside a bulk matrix. The results have been presented in terms of two types of matrices: (i) colloid-sized matrix particles (size ratio  $s = 1$ ) being a reference system and (ii) matrix particles which are much larger than the colloids (size ratio  $s = 50$ ). The case of small matrix particles is limited to relatively low packing fractions ( $\eta_m \sim 0.2$ ), whereas in the second

case, much higher matrix packing fractions are accessible ( $\eta_m \sim 0.5$ ), the pores of the matrix being much larger. Additionally, we have suggested that case (i) as well as (ii) could in principle be realized experimentally in 3D, i.e. using laser tweezers and colloidal sediments respectively, to serve as a model porous medium for colloidal suspensions.

We have shown that in the limit of infinitely large matrix particles, the standard AO results (without matrix) are recovered via a simple rescaling. In case of  $s = 50$  our bulk but also the interface results can be mapped onto the case without matrix with high accuracy. However, in the case of small matrix particles ( $s = 1$ ) this mapping fails, which is due to the more complex (and smaller) pore geometry on the colloidal scale.

Assuming a more “experimental” point of view, we have considered a tiny sample of porous matrix immersed in a large system of colloid-polymer mixture. When the fluid-fluid binodal is approached in the colloid-poor region of the phase diagram, capillary condensation occurs in the sample. This transition appears as a capillary line in the phase diagram (in system representation) extending along the binodal and ending in a capillary critical point. In case of small matrix particles, the capillary lines (for various densities of the matrix) are well separated from the bulk binodal but the capillary critical points lie deep into the colloidal gas regime. Concerning the large matrix particles, these capillary critical points are located closer to the bulk critical point, however, the capillary lines are also very close to the binodal. Still, using density-matched colloidal suspensions, we argue that capillary condensation may be observable in experiments.

We have computed fluid-fluid profiles inside the porous matrix as well as the corresponding surface tensions. For  $s = 50$ , these can be mapped onto the case without matrix but for  $s = 1$  the critical point shifts to higher polymer fugacities. Therefore, increasing the density of the matrix, profiles become smoother due to effective approach of the critical point. Solving the ROZ equations, we have also determined the crossover between monotonic and periodic decay of pair correlations of the mixture inside the matrix for  $s = 1$ . Comparing these with the decay of the interfacial correlations we find a small discrepancy which is probably due to numerical limits.

It should be noted that we do not expect our current approach to satisfactorily describe the (subtle) phenomena associated with wetting of the curved surfaces of the matrix particles by the colloidal liquid [60, 63]. Especially for  $s = 50$  close to the critical point in the complete wetting regime (of the planar hard wall), we can well imagine that the growths of thick wetting films preempt our capillary condensation transitions as well as disturb the fluid-fluid interfaces.

Concerning the fluid profiles, we have only considered a homogeneous background of matrix particles in this paper. It would be interesting to use inhomogeneous matrix realizations, as e.g. a step function of zero and nonzero matrix packing fraction (i.e. the interface of empty space-

matrix) or a constant matrix background in contact with a hard wall. Both types could give rise to interesting and substantially modified wetting behaviour. Additionally, one could also consider other types of matrices, e.g. quenched polymers or combinations of quenched colloids with quenched polymers [43, 51]. These are maybe less realistic from an experimental point of view but still interesting due to the competition of capillary condensation with evaporation.

As we have mentioned in the introduction, there are no experiments concerning phase behavior of colloidal suspensions in contact with 3D porous media to our knowledge. We hope that the accumulating results [7, 8, 9, 10, 11, 12, 43, 51], including those in this paper, may encourage more experimental efforts in that direction. It is important to keep in mind that a suitable porous matrix is a compromise between length scales: large enough to allow penetration of the colloids into the void space, but small enough to retain significant surface and capillary effects. In colloidal fluids in general, these last-mentioned effects are known to be much smaller than in atomic systems, thus providing a formidable challenge to experimentalists aiming to observe e.g. capillary condensation of a colloidal suspension in a porous matrix.

#### Acknowledgments

The authors would like to thank D. G. A. L. Aarts for useful discussions and R. Blaak for a critical read-

ing of the manuscript. MS thanks D. L. J. Vossen for detailed explanations of the laser-tweezer setup and T. Gisler for pointing out Refs. [7, 8]. This work is financially supported by the SFB-TR6 program ‘‘Physics of colloidal dispersions in external fields’’ of the *Deutsche Forschungsgemeinschaft* (DFG). The work of MS is part of the research program of the *Stichting voor Fundamenteel Onderzoek der Materie* (FOM), that is financially supported by the *Nederlandse Organisatie voor Wetenschappelijk Onderzoek* (NWO).

#### APPENDIX A: BULK FLUID FREE ENERGY

The bulk free energy of the colloid-polymer mixture in contact with a homogeneous hard-sphere porous matrix as given in Eq. (19) is

$$f(\eta_c, \eta_p, \eta_m) = \eta_c (\ln \eta_c - 1) + \frac{\eta_p}{q^3} (\ln \eta_p - 1) + f_0(\eta_c, \eta_m) - \frac{\eta_p}{q^3} \ln \alpha(\eta_c, \eta_m) \quad (\text{A1})$$

We note the occurrence of only third and lower powers of  $1/s$  in both  $f_0$  and  $\alpha$  which are given by

$$f_0(\eta_c, \eta_m) = \frac{\eta_m}{s^3} \ln(1 - \eta_m) - \left( \frac{\eta_m}{s^3} + \eta_c \right) \ln(1 - \eta_c - \eta_m) + \frac{3\eta_c \eta_m^2 (2 + \eta_c(\eta_m - 2) - 2\eta_m)}{2s^3(1 - \eta_m)^2(1 - \eta_c - \eta_m)^2} + \frac{3\eta_c}{2s^3(1 - \eta_c - \eta_m)^2} \{ \eta_m(2 - 2\eta_c + \eta_m)s + \eta_m(2 + \eta_c - 2\eta_m)s^2 + \eta_c(2 - \eta_c - 2\eta_m)s^3 \} \quad (\text{A2})$$

and

$$\ln \alpha(\eta_c, \eta_m) = \ln(1 - \eta_c - \eta_m) + \frac{q}{2s^3(1 - \eta_c - \eta_m)^3} \{ 2\eta_m(1 + \eta_c^2 + \eta_m + \eta_m^2 - \eta_c(2 + \eta_m))q^2 - 3\eta_m q [-2 + \eta_m + \eta_m^2 + 2\eta_c^2(-1 + q) - \eta_c(-4 + \eta_m + 2q + 4\eta_m q)] s + 6\eta_m [(1 - \eta_c - \eta_m)^2 + 3\eta_c(1 - \eta_c - \eta_m)q + \eta_c(1 + 2\eta_c - \eta_m)q^2] s^2 + \eta_c [-\eta_c(1 - \eta_m)(12 + (3 - 2q)q) + 2(1 - \eta_m)^2(3 + q(3 + q)) + \eta_c^2(6 + q(-3 + 2q))] s^3 \}. \quad (\text{A3})$$

[1] R. Evans, *J. Phys.: Condens. Matter* **2**, 8989 (1990).

[2] L. D. Gelb, K. E. Gubbins, R. Radhakrishnan, and M. Sliwiska-Bartkowiak, *Rep. Prog. Phys.* **62**, 1573 (1999).

[3] R. G. Smith and G. C. Maitland, *Trans. IChemE.* **76A**, 539 (1998).

[4] R. Hilfer, in *Statistical Physics and Spatial Statistics*,

- Vol. 554 of *Springer Lecture Notes in Physics*, edited by K. R. Mecke and D. Stoyan (Springer, Berlin, 2000), p. 203.
- [5] K. R. Mecke, *Physica A* **314**, 655 (2002).
- [6] H. Löwen, *J. Phys.: Condens. Matter* **13**, R415 (2001).
- [7] G. Cruz de León, J. M. Saucedo-Solorio, and J. L. Arauz-Lara, *Phys. Rev. Lett.* **81**, 1122 (1998).
- [8] G. Cruz de León and J. L. Arauz-Lara, *Phys. Rev. E* **59**, 4203 (1999).
- [9] S. G. J. M. Kluijtmans, J. K. G. Dhont, and A. P. Philipse, *Langmuir* **13**, 4982 (1997).
- [10] S. G. J. M. Kluijtmans and A. P. Philipse, *Langmuir* **15**, 1896 (1999).
- [11] S. G. J. M. Kluijtmans, G. H. Koenderink, and A. P. Philipse, *Phys. Rev. E* **61**, 626 (2000).
- [12] P. Weroński, J. Y. Walz, and M. Elimelech, *J. Coll. Int. Sci.* **262**, 372 (2003).
- [13] J. P. Hoogenboom, D. L. J. Vossen, C. Faivre-Moskalenko, M. Dogterom, and A. van Blaaderen, *Appl. Phys. Lett.* **80**, 4828 (2002).
- [14] W. C. K. Poon, *J. Phys.: Condens. Matter* **14**, R859 (2002).
- [15] S. Asakura and F. Oosawa, *J. Chem. Phys.* **22**, 1255 (1954).
- [16] S. Asakura and F. Oosawa, *J. Polym. Sci.* **33**, 183 (1958).
- [17] A. Vrij, *Pure and Appl. Chem.* **48**, 471 (1976).
- [18] A. P. Gast, C. K. Hall, and W. B. Russell, *J. Coll. Int. Sci.* **96**, 251 (1983).
- [19] M. Dijkstra, J. M. Brader, and R. Evans, *J. Phys.: Condens. Matter* **11**, 10079 (1999).
- [20] H. N. W. Lekkerkerker, W. C. K. Poon, P. N. Pusey, A. Stroobants, and P. B. Warren, *Europhys. Lett.* **20**, 559 (1992).
- [21] M. Schmidt, H. Löwen, J. M. Brader, and R. Evans, *Phys. Rev. Lett.* **85**, 1934 (2000).
- [22] M. Schmidt, H. Löwen, J. M. Brader, and R. Evans, *J. Phys.: Condens. Matter* **14**, 9353 (2002).
- [23] P.G. Bolhuis, A.A. Louis, J.P. Hansen, *Phys. Rev. Lett.* **89**, 128302 (2002).
- [24] M. Dijkstra and R. van Roij, *Phys. Rev. Lett.* **89**, 208303 (2002).
- [25] A. Vrij, *Physica A* **235**, 120 (1997).
- [26] J. M. Brader and R. Evans, *Europhys. Lett.* **49**, 678 (2000).
- [27] J. M. Brader, R. Evans, M. Schmidt, and H. Löwen, *J. Phys.: Condens. Matter* **14**, L1 (2002).
- [28] J. M. Brader, Ph.D. thesis, University of Bristol, 2001.
- [29] I. O. Götze, J. M. Brader, M. Schmidt, and H. Löwen, *Mol. Phys.* **101**, 1651 (2003).
- [30] E. H. A. de Hoog and H. N. W. Lekkerkerker, *J. Phys. Chem. B* **103**, 5274 (1999).
- [31] E. H. A. de Hoog, H. N. W. Lekkerkerker, J. Schulz, and G. H. Findenegg, *J. Phys. Chem. B* **103**, 10657 (1999).
- [32] E. H. A. de Hoog, Dissertation, Utrecht University, 2001.
- [33] D. G. A. L. Aarts, J. H. van der Wiel, and H. N. W. Lekkerkerker, *J. Phys.: Condens. Matter* **15**, S245 (2003).
- [34] D. G. A. L. Aarts and H. N. W. Lekkerkerker, private communication (unpublished).
- [35] W. K. Wijting, N. A. M. Besseling, and M. A. Cohen Stuart, *Phys. Rev. Lett.* **90**, 196101 (2003).
- [36] R. Evans, in *Fundamentals of Inhomogeneous Fluids*, edited by D. Henderson (Dekker, New York, 1992), p. 85.
- [37] L. J. D. Frink, A. G. Salinger, M. P. Sears, J. D. Weinhold, and A. L. Frischknecht, *J. Phys.: Condens. Matter* **14**, 12167 (2002).
- [38] A. G. Salinger and L. J. D. Frink, *J. Chem. Phys.* **118**, 7457 (2003).
- [39] L. J. D. Frink and A. G. Salinger, *J. Chem. Phys.* **118**, 7466 (2003).
- [40] E. Kierlik, P. A. Monson, M. L. Rosinberg, L. Sarkisov, and G. Tarjus, *Phys. Rev. Lett.* **87**, 055701 (2001).
- [41] E. Kierlik, P. A. Monson, M. L. Rosinberg, and G. Tarjus, *J. Phys.: Condens. Matter* **14**, 9295 (2002).
- [42] M. L. Rosinberg, E. Kierlik, and G. Tarjus, *Europhys. Lett.* **62**, 377 (2003).
- [43] M. Schmidt, *Phys. Rev. E* **66**, 041108 (2002).
- [44] Y. Rosenfeld, *Phys. Rev. Lett.* **63**, 980 (1989).
- [45] Y. Rosenfeld, M. Schmidt, H. Löwen, and P. Tarazona, *Phys. Rev. E* **55**, 4245 (1997).
- [46] P. Tarazona, *Phys. Rev. Lett.* **84**, 694 (2000).
- [47] W. G. Madden and E. D. Glandt, *J. Stat. Phys.* **51**, 537 (1988).
- [48] W. G. Madden, *J. Chem. Phys.* **96**, 5422 (1992).
- [49] J. A. Given and G. Stell, *J. Chem. Phys.* **97**, 4573 (1992).
- [50] J. A. Given and G. R. Stell, *Physica A* **209**, 495 (1994).
- [51] M. Schmidt, E. Schöll-Paschinger, J. Köfinger, and G. Kahl, *J. Phys.: Condens. Matter* **14**, 12099 (2002).
- [52] M. Schmidt, to appear in *Phys. Rev. E* (unpublished).
- [53] M. Schmidt and J. M. Brader, to appear in *J. Chem. Phys.* (unpublished).
- [54] L. Lafuente and J. A. Cuesta, *Phys. Rev. Lett.* **89**, 145701 (2002).
- [55] M. Schmidt, L. Lafuente, and J. A. Cuesta, to appear in *J. Phys.: Condens. Matter* (unpublished).
- [56] P. I. Ravikovitch, A. Vishnyakov, and A. V. Neimark, *Phys. Rev. E* **64**, 011602 (2001).
- [57] S. Figueroa-Gerstenmaier, F. J. Blas, J. B. Avalos, and L. F. Vega, *J. Chem. Phys.* **118**, 830 (2003).
- [58] A. Trokhymchuk and S. Sokolowski, *J. Chem. Phys.* **109**, 5044 (1998).
- [59] J. Reszko-Zygmunt, A. Patrykiewicz, S. Sokolowski, and Z. Sokolowska, *Mol. Phys.* **100**, 1905 (2002).
- [60] R. Evans, R. Roth, and P. Bryk, *Europhys. Lett.* **62**, 815 (2003).
- [61] R. Evans, R. J. F. Leote de Carvalho, J. R. Henderson, and D. C. Hoyle, *J. Chem. Phys.* **100**, 591 (1994).
- [62] J. M. Brader, A. Esztermann, and M. Schmidt, *Phys. Rev. E* **66**, 031401 (2002).
- [63] R. Roth and R. Evans, private communication (unpublished).